A THREE DIMENSIONAL FINITE VOLUME APPROACH TO THE THERMO-MECHANICAL MODELLING OF THE SHAPE CASTING OF METALS

G. A. Taylor, C. Bailey and M. Cross

Centre for Numerical Modelling and Process Analysis,
University of Greenwich,
London SE18 6PF, UK.
E-mail : G.A.Taylor@gre.ac.uk

Abstract

This paper presents a three dimensional, thermo-mechanical modelling approach to the cooling and solidification phases associated with the shape casting of metals ie. die, sand and investment casting. Novel vertex-based Finite Volume (FV) methods are described and employed with regard to the small strain, non-linear Computational Solid Mechanics (CSM) capabilities required to model shape casting. The CSM capabilities include the non-linear material phenomena of creep and thermo-elasto-visco-plasticity at high temperatures and thermo-elasto-plasticity at low temperatures and also multi-body deformable contact which can occur between the metal casting and the mould. The vertex-based FV methods, which can be readily applied to unstructured meshes, are included within a comprehensive FV modelling framework, PHYSICA. The additional heat transfer, by conduction and convection, filling, porosity and solidification algorithms existing within PHYSICA for the complete modelling of all shape casting processes employ cell-centred FV methods. The thermo-mechanical coupling is performed in a staggered incremental fashion, which addresses the possible gap formation between the component and the mould, and is ultimately validated against a variety of shape casting benchmarks.

Introduction

Over the last 10 to 15 years a large research effort has been employed in the development of physically accurate software tools for the complete simulation of the shape casting process [1, 12], with the ultimate aim of providing a core design tool for the foundry engineer. To be of major use to the foundry engineer the simulation software must be tolerably accurate within a reasonable computational time. This generally requires a flexible software framework which can be extended in a modular fashion depending upon the physical nature of the particular casting simulation required [1, 2]. In this research, the 3D FV framework PHYSICA [13] is employed and the inclusion of the CSM capabilities required for the complete modelling of the thermo-mechanical behaviour is described. The numerical methods for the solution of the heat transfer, fluid flow, filling and porosity formation employ cell-centred FV procedures and have been included within the PHYSICA framework [1, 3, 13]. A description of these procedures is provided elsewhere [1, 3]. With regard to the CSM capabilities, material models which furnish the temperature dependent constitutive behaviour exhibited by metals between the extremes of the solidifying range and room temperatures are required. Recently, two and three dimensional vertex-based FV procedures have been employed in the numerical solution of problems involving rate dependent and rate independent plasticity and reasonable comparisons have been obtained against the standard Galerkin finite element method with regard to both numerical accuracy and computational efficiency [11]. These procedures have been encapsulated within the PHYSICA framework to provide complete simulation of the shape casting process [11]. Additionally, CSM procedures for frictional contact between the solidifying component and associated mould are required. At present a vertex-based FV procedure is being developed within the PHYSICA framework, which employs an augmented Lagrangian technique with regard to the contact constraints [14].

Computational Solid Mechanics

A treatment for frictional contact is outlined by considering the displacement of two deformable bodies as described in Figure 1(a). In this illustrative problem it is assumed that the bodies (1) and (2), slave and master respectively, are not initially in contact, but in subsequent configurations $\{x\}^{(i)} = \{u\}^{(i)}(\{X\}^{(i)})$ the two bodies are in contact within the designated boundary regions $\gamma^{(i)}$. Although this description is limited to two bodies, it will apply generally to multi-body contact problems by accounting for each contacting pair consecutively.

(a)

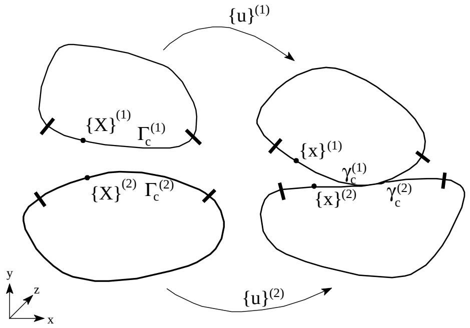

(b)

$$\boxed{\begin{array}{lcll} g(\{X\}^{(1)}) & \leq & 0, & \text{(i)} \\ t_n(\{X\}^{(1)}) & \geq & 0, & \text{(ii)} \\ t_n(\{X\}^{(1)})g(\{X\}^{(1)}) & = & 0, & \text{(iii)} \\ t_n(\{X\}^{(1)})\dot{g}(\{X\}^{(1)}) & = & 0 & \text{(iv).} \end{array}}$$

Figure 1: Frictional contact, (a) the two-body model and (b) Kuhn-Tucker constraints.

Gap Function and Contact Constraints

Any slave point $\{X\}^{(1)}$ that belongs to the contacting boundary $\Gamma_c^{(1)}$ is considered to have a gap distance from the master surface $\Gamma_c^{(2)}$. The displacement $\{u\}^{(1)}(\{X\}^{(1)})$ is admissible if there is no penetration of the slave point into the master body and the gap function is defined as follows:

$$g(\{X\}^{(1)}) = \text{sign}(g(\{X\}^{(1)}))\left|g(\{X\}^{(1)})\right|, \tag{1}$$

where

$$\left|g(\{X\}^{(1)})\right| = \left|\left|\{u\}^{(1)}(\{X\}^{(1)}) - \mathrm{proj}_{\gamma_c^{(2)}}(\{u\}^{(1)}(\{X\}^{(1)}))\right|\right| \tag{2}$$

and

$$\mathrm{sign}(g(\{X\}^{(1)})) = \begin{cases} -1 & \text{if } \{u\}^{(1)}(\{X\}^{(1)}) \text{ is admissible,} \\ +1 & \text{otherwise.} \end{cases} \tag{3}$$

This definition of $g(\{X\}^{(1)})$ is given in terms of the closest point projection (proj) of $\{x\}^{(1)} = \{u\}^{(1)}(\{X\}^{(1)})$ onto $\gamma_c^{(2)}$. The Kuhn-Tucker constraints for contact are described in Figure 1(b), where, inequality (i) is the impenetrability constraint, inequality (ii) is the normal traction (compressive) constraint, equality (iii) is the requirement that the pressure is non-zero only when $g(\{X\}) = 0$ and equality (iv) is the persistency condition which is applied when considering frictional kinematics.

Equilibrium Equations and Boundary Conditions

In matrix form, the incremental equilibrium equations are

$$[L]^T\{\Delta\sigma\}^{(i)} + \{b\}^{(i)} = \{0\} \qquad \text{in } \Omega^{(i)}, \tag{4}$$

where $[L]$ is the differential operator, $\{\Delta\sigma\}^{(i)}$ is the Cauchy stress, $\{b\}^{(i)}$ is the body force and $\Omega^{(i)}$ is is the domain, all relating to body (i). The boundary conditions on the surface $\Gamma^{(i)} = \Gamma_t^{(i)} \cup \Gamma_u^{(i)}$ of the domain $\Omega^{(i)}$ can be defined as [15, 8]

$$\begin{aligned} [R]^T\{\sigma\}^{(i)} &= \{t_p\}^{(i)} \qquad \text{on } \Gamma_t^{(i)} \text{ and} && (5) \\ \{u\}^{(i)} &= \{u_p\}^{(i)} \qquad \text{on } \Gamma_u^{(i)}, && (6) \end{aligned}$$

where $\{t_p\}^{(i)}$ are the prescribed tractions on the boundary $\Gamma_t^{(i)}$, $\{u_p\}^{(i)}$ are the prescribed displacements on the boundary $\Gamma_u^{(i)}$ and $[R]$ is the outward normal operator [11].

Constitutive Relationship

In matrix form, the incremental stress is related to the incremental elastic strain as follows; $\{\Delta\sigma\} = [D]\{\Delta\epsilon_e\}$, where $[D]$ is the elasticity matrix. For the deformation of metals, the von-Mises yield criterion is employed and the incremental elastic strain is given by $\{\Delta\epsilon_e\} = \{\Delta\epsilon\} - \{\Delta\epsilon_t\} - \{\Delta\epsilon_{vp}\}$, where $\{\Delta\epsilon\}$, $\{\Delta\epsilon_t\}$ and $\{\Delta\epsilon_{vp}\}$ are the total, thermal and visco-plastic incremental strain, respectively. The visco-plastic strain rate is given by the Perzyna [9] model

$$\frac{d}{dt}\{\epsilon_{vp}\} = \gamma\left\langle \frac{\sigma_{eq}}{\sigma_y} - 1 \right\rangle^{\frac{1}{N}} \frac{3}{2\sigma_{eq}}\{s\}, \tag{7}$$

where σ_{eq}, σ_y, γ, N and s are the equivalent stress, yield stress, fluidity, strain rate sensitivity parameter and deviatoric stress, respectively. The $< x >$ operator is defined as follows:

$$< x > = \begin{cases} 0 & \text{when} \quad x \leq 0 \quad \text{and} \\ x & \text{when} \quad x > 0. \end{cases}$$

The incremental total strain for infinitesimal strains is $\{\Delta\epsilon\} = [L]\{\Delta u\}$, where $\{\Delta u\}$ is the incremental displacement.

Vertex-based Discretisation

Employing the method of weighted residuals to equations (4), (5) and (6) and considering the contact constraints $\{t_c\}^{(i)}$, it is possible to obtain the following weak form of the equilibrium equation;

$$\begin{aligned} &- \int_\Omega [LW]^T\{\Delta\sigma\}^{(i)}\,d\Omega + \int_\Omega [W]^T\{b\}^{(i)}\,d\Omega + \int_{\Gamma_u} [RW]^T\{\Delta\sigma\}^{(i)}\,d\Gamma + \int_{\Gamma_t} [W]^T\{t_p\}^{(i)}\,d\Gamma \\ &- \int_{\Gamma_c} [W]^T\{t_c\}^{(i)}\,d\Gamma \;=\; \{0\}, \qquad (8) \end{aligned}$$

where $[W]$ is a diagonal matrix of arbitrary weighting functions. The standard virtual work formulation can be obtained by replacing $[W]$ with a vector of virtual displacements and as the weighting functions are arbitrary it is possible to obtain the FV formulation by assuming unit virtual displacements, such that

$$\Phi(\{\Delta u\}^{(i)}) = \int_{\Gamma_u} [R]^T \{\Delta\sigma\}^{(i)} d\Gamma + \int_{\Omega} \{b\}^{(i)} d\Omega + \int_{\Gamma_p} \{t_p\}^{(i)} d\Gamma = \int_{\Gamma_c} \{t_c\}^{(i)} d\Gamma. \tag{9}$$

More directly, the weighting function matrix can be assumed equal to the identity matrix [I], which is equivalent to the sub-domain collocation technique [8, 15]. The FV formulation applies generally regardless of the constitutive relationship employed. In this research the constitutive relationship as described previously is employed [11]. The solution of the constrained equation (9) is an optimisation problem and requires solution schemes which convert the problem to an unconstrained one, in this research an augmented Lagrangian technique has been employed [14]. Shape functions are utilised in the standard fashion to furnish the variation of displacements and derivatives over the mesh elements [11]. The control volumes over which equation (9) is integrated are based around the vertices of the mesh and are constructed from sub-control volume contributions from the associated elements as illustrated in Figure 2(a) [11].

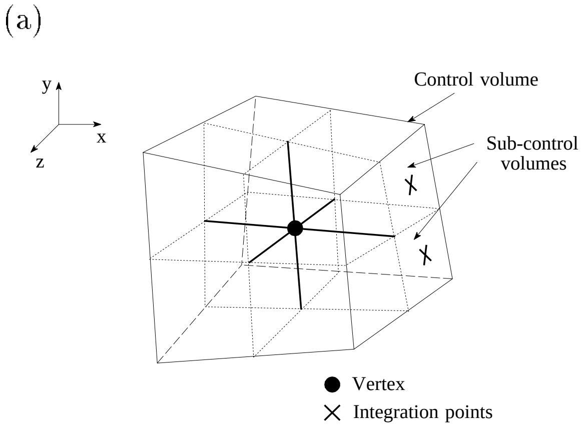

(b)

1. Solve heat transfer and phase change.
2. Solve CSM due to thermal load.
3. Recalculate geometrical quantities.
4. Repeat 1-3 for next time interval.

Figure 2: (a) 3D vertex-based control volume and (b) incremental solution approach.

The resulting non-linear system of discretised equations are of the form $[K]\{\Delta\bar{u}\} - \{f\} = \{0\}$, where $[K]$ is the system matrix, $\{\Delta\bar{u}\}$ is the incremental displacement vector at the nodes and $\{f\}$ is the load vector. It should be noted that the same mesh is employed throughout the analysis in PHYSICA [13] to represent the domains in question and to generate the control volumes.

Dual Thermo-mechanical Coupling

During the shape casting process coupled thermo-mechanical behaviour occurs. The molten metal is initially in contact with the mould and a thermal resistance can be associated with the casting/mould interface due to the rugosity of the mould surface [10]. As the casting solidifies, gap formation can occur at the interface and the thermal resistance will increase as a function of the gap. The thermo-mechanical coupling is performed in a staggered incremental fashion as illustrated in Figure 2(b).

Thermal Boundary Conditions at the Casting/mould Interface

The gap formation is tracked via coincident nodes at the casting/mould interface, consequently the cell faces at the interface are initially coincident [5]. The heat transfer flux is calculated at the centre of the cell faces and updated as the gap develops. This is reasonable for problems involving small strains as the face connectivities are not drastically altered due to the mechanical deformation. An equivalent gap g_{eq} can be associated with the thermal contact resistance [10] $1/h_{\text{cr}} = g_{\text{eq}}/k_{\text{cr}}$, where k_{cr} is the thermal conductivity associated with the interface, initially. The complete thermal behaviour of the interface can be implemented using [7]

$$\frac{\partial T}{\partial n} = h_{\text{eff}} \left(T_{\text{casting}} - T_{\text{mould}} \right), \tag{10}$$

where the effective heat transfer coefficient at the interface is a function of the effective air gap g_{ag}, such that [10]

$$h_{\text{eff}} = \begin{cases} h_{\text{cr}} & \text{when } g_{\text{ag}} \leq g_{\text{eq}} \text{ and} \\ \frac{k_{\text{ag}}}{g_{\text{ag}}} & \text{when } g_{\text{ag}} > g_{\text{eq}}, \end{cases} \tag{11}$$

where k_{ag} is the conductivity of the air gap. It is important to note that the heat transfer across the interface is not necessarily a purely conductive process. Consequently, an effective conductivity associated with the air gap can be utilised to facilitate this behaviour. This requires accurate experimental measurement of the heat transfer coefficient as a function of the gap [10, 4].

Results and Discussion

In the following simulations the moulds are in an initially full state with regard to the molten metal and uniform temperatures in the casting domains are assumed. The first test case compares numerical predictions with experimental results [10] for the die casting of a hollow aluminium cylinder. Figure 4(a) illustrates the experimental design, where the top and bottom of the cylinder and dies are insulated to ensure a predominantly radial heat loss. Thermocouples were inserted into the cylinder and dies, and a displacement transducer was attached to the cylinder to monitor the gap formation at the cylinder/die interface. A fully coupled analysis was performed in PHYSICA [13] to simulate the cooling, solidification and resulting mechanical deformation of the cylinder [11]. The material properties of the aluminium casting, steel dies and insulation are given in Figures 5(a), (b) and (c), respectively. The heat transfer coefficient h_{eff} was assumed to vary linearly between $400\text{W/m}^2\text{K}$ to $20\text{W/m}^2\text{K}$ corresponding to gap distances of 0.0 to 0.5 mm, based upon experimental results [10]. The mesh employed in the numerical analysis is described in Figure 3(a). Figure 4(b) illustrates the predicted deformation of the aluminium cylinder at several instances in time. As expected, the cylinder contracts away from the external die and against the internal core, creating gaps at the top and external interfaces. Figure 6(a) compares predicted cooling rates, with and without gap formation, for both the cylinder and external die against those obtained from experimental readings. The upper cooling rates are recorded at a location in the casting close to the external die [10]. For a thermo-mechanical analysis including

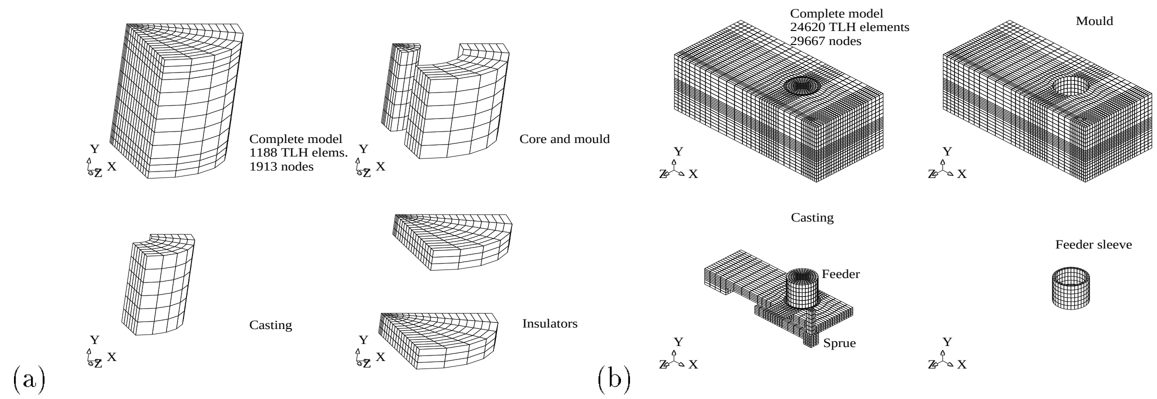

Figure 3: Meshes employed in the analysis of, (a) die and (b) sand casting.

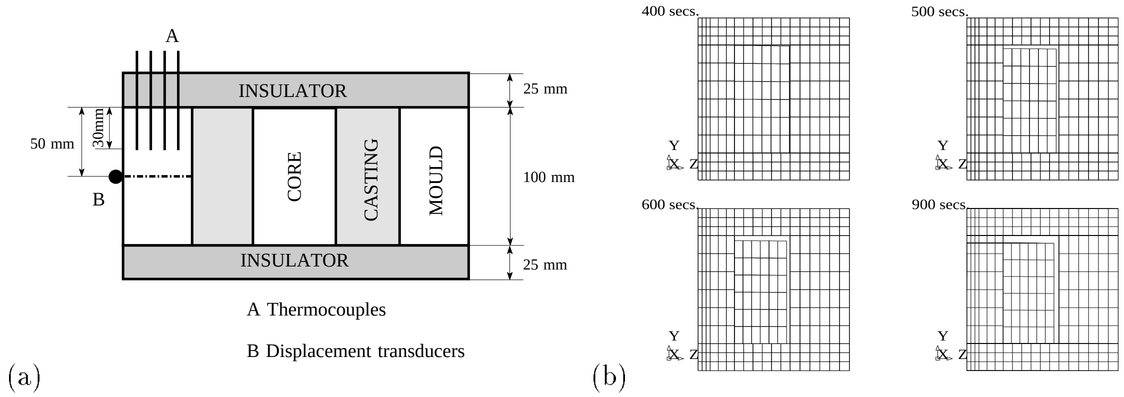

Figure 4: Die casting of a cylinder, (a) experimental analysis and (b) simulated deformation.

T_L	Liquidus temp.	618.8°C	
T_S	Solidus temp.	566.4°C	
h	Latent heat	440 kJ/kg	
k	Conductivity	150 W/(mK)	
ρ	Density	2,710 kg/m^3	
c	Specific heat	1,160 J/(kgK)	
α	Thermal expansion	5×10^{-5}/K	
ν	Poisson's ratio	0.33	
E	Young's modulus	60,000MPa	20°C
		34,000MPa	450°C
		10^{-2}MPa	566.4°C
Y	Yield stress	500MPa	20°C
		10^{-4}MPa	566.4°C

(a)

k	Conductivity	33 W/(mK)
ρ	Density	7,880 kg/m^3
c	Specific heat	600 J/(kgK)

(b)

k	Conductivity	0.1 W/(mK)
ρ	Density	1,000 kg/m^3
c	Specific heat	1,760 J/(kgK)

(c)

Figure 5: Material property tables, (a) aluminium (b) steel and (c) insulation.

contraction and associated gap formation, the results are in closer agreement with the experimental readings. The lower cooling rates are for a location in the external die and are also in closer agreement for a thermo-mechanical analysis. In summary, with regard to die casting, neglecting of the gap formation at the casting/die interface will affect the cooling rates and consequently the casting solidification. Figure 6(b) shows the resulting gap formation at the centre of the cylinder/external die interface over time. Again, the predictions compare reasonably well with the experimental readings. It is important to note that rate dependent and rate independent analyses were performed for the die casting problem, where rapid cooling rates are observed, and negligible variation of results was observed. This may indicate that more accurate material properties are required with regard to rate dependency or that viscous effects are negligible due to the rapid cooling [6].
The next simulation is a fully three dimensional sand casting and the mesh employed is described in Figure 3(b). In this simulation heat transfer, fluid flow, solidification and solid mechanics are fully coupled. Figure 7(b) illustrates the amount of thermal convection in the initial stages of cooling. It is interesting to note the large recirculatory flow in the feeder region. This is expected as an insulating material has been placed around the feeder to ensure that it remains in a liquid state

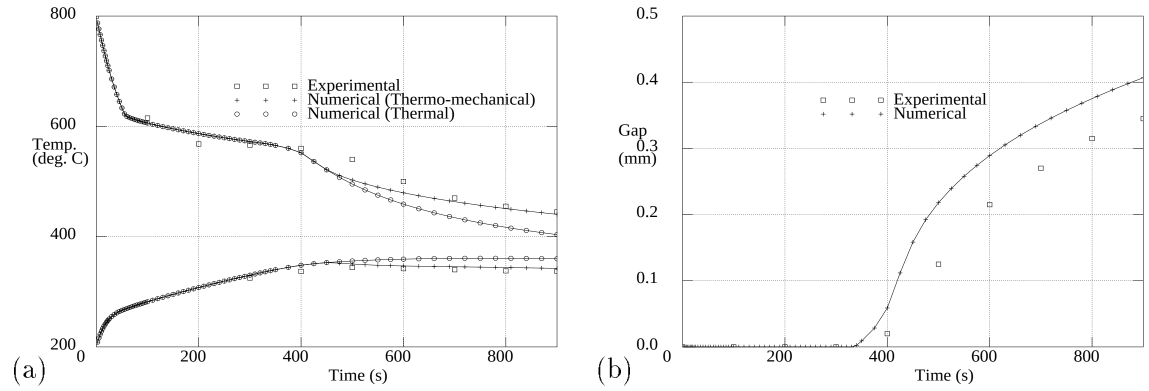

Figure 6: Simulated die casting of a cylinder, (a) temperature profiles and (b) gap formation.

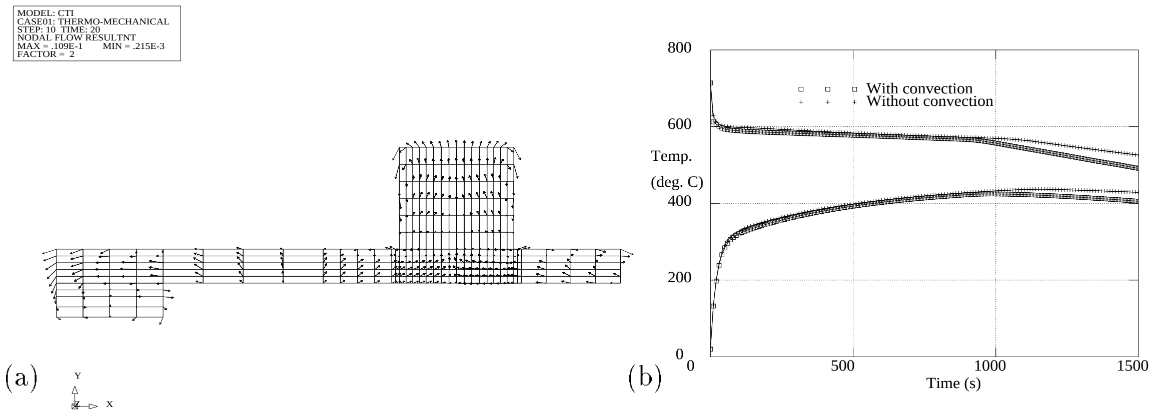

Figure 7: Simulated sand casting of a test bar, (a) convection and (b) temperature profiles.

and can feed areas of the casting which are prone to shrinkage porosity. The effect of convection on the cooling rates was investigated. Figure 7(b) shows the differences in cooling rates for analyses with and without convection. Differences of approximately 50^oC can be observed, where thermal convection in the molten metal promotes redistribution of heat, hence raising temperatures near the interface and therefore resulting in faster cooling rates. Alternatively, it is important to note that because of the thermal gradients associated with the geometry of the die casting problem the cooling rates are unaffected by the consideration of natural convection [11].

Conclusions

At present, deformable and rigid contact analyses between casting and mould have been performed. Neglecting mould dilation affects the accuracy of the gap prediction in the die casting problem. The multi-body deformable contact approach described in this paper will be implemented shortly and will furnish gap predictions of greater accuracy. The residual convection, which is possible in shape casting, is dependent upon the thermal gradients associated with the casting geometry, the mould filling and subsequent feeding if applicable. Further research is underway in these areas to provide a more accurate prediction of the cooling rates observed in shape casting [3]. With regard to the computational effort required for a full thermo-mechanical analysis, the die casting problem required several hours whilst the sand casting problem required several days on a 143 MHz Sun ULTRASPARC processor. Ultimately, a fully coupled thermo-mechanical capability will be available within PHYSICA [13] to efficiently model the shape casting of metals on high performance computational platforms.

Acknowledgements

The financial assistance of the EPSRC, British Aerospace and Normalair-Garrett Ltd is acknowledged in this research.

References

[1] M. Cross. Development of novel computational techniques for the next generation of software tools for casting simulation. In T. S. Piwonka, V. Voller, and L. Katgerman, editors, *Modeling of Casting, Welding and Advanced Solidification Processes VI*, pages 115–126, 1993.

[2] C. Bailey et al. Multiphysics modelling of the metals casting process. In *Proc. R. Soc. Lond. A*, volume 452, pages 459–486, 1996.

[3] K.A. Pericleous et al. Integrated numerical modelling of the complete casting process. In M. P. Schwarz, M. R. Davidson, and A. K. Easton, editors, *Minerals & Metals Processing & Power Generation*, pages 321–328, 1997.

[4] M. Bellet et al. Thermomechanics of the cooling stage in casting processes: Three-dimensional finite element analysis and experimental validation. *Metallurgical and Materials Transactions B*, 27B:81–99, 1996.

[5] Y.D. Fryer. *A Control Volume Unstructured Grid Approach to the Solution of the Elastic Stress-Strain Equations.* PhD thesis, The University of Greenwich, 1993.

[6] H. G. Landau, J. H. Weiner, and E. E. Zwicky. Thermal stress in a viscoelastic-plastic plate with temperature dependent yield stress. *J. of Appl. Mech.*, 27:297–302, 1960.

[7] R. W. Lewis and P. M. Roberts. Finite element simulation of solidification problems. In T. J. Smith, editor, *Modelling of Flow and Solidification of Metals*, pages 61–92, 1987.

[8] E. Onate, M. Cervera, and O.C. Zienkiewicz. A finite volume format for structural mechanics. *Int. Journal for Num. Methods in Engg.*, 37:181–201, 1994.

[9] P. Perzyna. Fundamental problems in visco-plasticity. *Advan. Appl. Mech.*, 9:243–377, 1966.

[10] P. Schmidt and I. L. Svensson. Heat transfer and air gap formation in permanent mould casting of aluminium alloys. Technical Report TRITA-MAC-0541, Materials research centre, The royal institute of technology, S10044 Stockholm 70, 1994.

[11] G.A. Taylor. *A Vertex Based Discretisation Scheme Applied to Material Non-Linearity within a Multi-Physics Finite Volume Framework.* PhD thesis, The University of Greenwich, 1996.

[12] B. G. Thomas. Stress modelling of casting processes: An overview. In T. S. Piwonka, V. Voller, and L. Katgerman, editors, *Modeling of Casting, Welding and Advanced Solidification Processes VI*, pages 519–534, 1993.

[13] University of Greenwich, London, UK. (http://physica.gre.ac.uk/). *PHYSICA*.

[14] P. Wriggers, J.C. Simo, and R.L. Taylor. Penalty and augmented Lagrangian formulations for contact problems. In *Proceedings of the NUMETA '85 Conference (7-11 January)*, 1985.

[15] O.C. Zienkiewicz and R.L. Taylor. *The Finite Element Method: Volume 1: Basic Formulation and Linear Problems.* Magraw-Hill, Maidenhead, Berkshire, UK, 1989.